Modified TAB Model for Viscous Fluids applied to Breakup in Rotary Bell Spray Painting

B. Andersson*[1], V. Golovitchev[2], S. Jakobsson[1], A. Mark[1], F. Edelvik[1], L. Davidson[2], J. S. Carlson[1]
[1]Fraunhofer-Chalmers Centre, Chalmers Science Park, Göteborg, Sweden
[2]Department of Applied Mechanics, Chalmers University of Technology, Göteborg, Sweden
bjorn.andersson@fcc.chalmers.se, valeri@chalmers.se, stefan.jakobsson@fcc.chalmers.se, andreas.mark@fcc.chalmers.se, fredrik.edelvik@fcc.chalmers.se, lada@chalmers.se, johan.carlson@fcc.chalmers.se

Abstract

The Taylor Analogy Breakup (TAB) model is applied to droplet breakup in rotary bell spray painting commonly used in the automotive industry. The bell spins rapidly around its axis with a tangential velocity at the edge in the order of 100 m/s. The paint falls off the edge and enters the air with a large relative velocity, driving the atomization. The paint is a viscous fluid and a modification of the TAB model taking non-linear effects of large viscosity into account is described. The parameters in the breakup model are tuned to match droplet size distributions obtained in CFD simulations with measured ones. Results are presented for three cases with rotation speeds from 30 to 50 thousand RPM where the full droplet size distributions are compared with measurements. Good results are obtained for all three cases where the simulated size distributions compare well to measurements over a wide range of droplet sizes. The obtained results can be used in a preprocessing stage of a full spray painting simulation thereby reducing the need for costly and cumbersome measurements.

Introduction

In the automotive industry paint primer, color layers and clear coating are sprayed either with classical Pneumatic spray guns or using the Electrostatic Rotary Bell Sprayer (ERBS) technique. The focus here is on the rotating bell technique where paint is injected at the center of a rotating bell and is atomized at its edge. An image of an active bell is shown in Fig. 1.

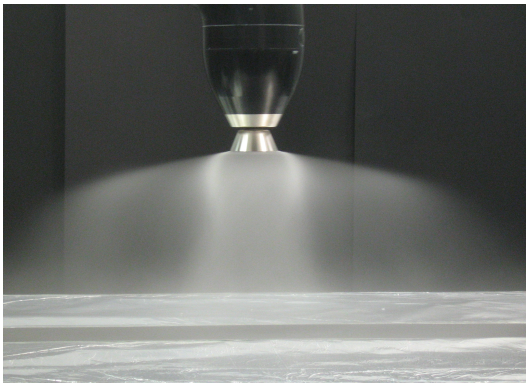

Figure 1. Photograph of rotary bell spraying towards a target. The actual bell is the cone shaped part at the tip of the applicator head. Courtesy of Swerea IVF.

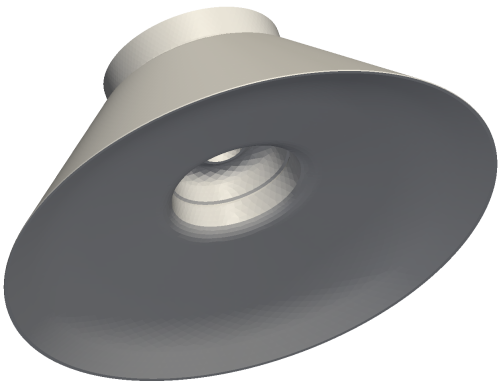

Figure 2. Bell geometry. The bell rotates around its axis and paint is transferred from the center to the edge by the centrifugal force.

The droplet size distribution of the spray determines its characteristics of how it reacts to the external forces applied by the air and the electrostatic field: large droplets tend to travel in straight lines and small droplets follow the force field closely. It is therefore important to have good knowledge about which distribution of sizes there is within the spray in order to be able to perform spray painting simulations with high accuracy. If a better understanding is gained on how the process parameters affect the distributions this can also be used to tune the result in order to have a better painting result and higher transfer efficiency.

*Corresponding author: bjorn.andersson@fcc.chalmers.se

Breakup has been studied in many contexts and one of the largest is probably combustion engine research. In a modern diesel or gasoline engine the fuel is injected through a nozzle with high pressure causing the atomization. The TAB model [1] was originally derived to model diesel injection where the penetration depth of the fuel and the average droplet size were compared to measurements. The model has since then been included in several software packages such as KIVA [2] and OpenFOAM [3].

The aim of this paper is to investigates the ability of the TAB model to predict the paint size distributions by varying the process parameters. The model is implemented in the flow solver IBOFlow [4] which is part of the larger solver framework IPS Virtual Paint used to simulate the spray painting in the automotive industry with the rotary bell technique [5, 6]. By being able to simulate the droplet breakup the need for costly and cumbersome measurements is reduced. The obtained results are then used as input to full spray painting simulations that can be used in the automotive industry to reduce the time required for introduction of new car models, reduce the environmental impact and increase the quality.

Problem description

Taylor Analogy Breakup (TAB) model

The Taylor Analogy Breakup (TAB) model [1] is based on the fundamental mode of oscillation of a sphere. The sphere is modeled as a damped harmonic oscillator where the driving force is the relative motion to the surrounding medium, the restoring force is the surface tension, and the damping comes from the viscosity of the fluid inside the droplet. The reader is referred to the original paper [1] for a complete derivation, but some steps are reproduced here.

The equation for a damped harmonic oscillator can be written as

$$m_p\ddot{x} = F - kx - d\dot{x}, \tag{1}$$

where x is the displacement of the equator of the droplet from its equilibrium position, m_p is the droplet mass, F is the driving force, k is the spring constant, and d is the damping coefficient. The Taylor analogy identifies the following relations for the coefficients,

$$\frac{F}{m_p} = C_F\frac{\rho_g u_r^2}{\rho_l a}, \qquad \frac{k}{m_p} = C_k\frac{\sigma}{\rho_l a^3}, \qquad \frac{d}{m_p} = C_d\frac{\mu_l}{\rho_l a^2}, \tag{2}$$

where ρ_g and ρ_l are the gas and liquid densities, respectively, u_r is the modulus of the relative velocity between the droplet and the surrounding medium, a is the droplet radius, σ is the surface tension, and μ_l is the liquid viscosity.

The three expressions are derived from the dynamic pressure, the surface tension force and the viscous force, respectively. The dynamic pressure is expressed as $\rho_g u_r^2/2$ and is integrated over the projected area of the droplet resulting in a full expression for the force proportional to $\rho_g u_r^2 a^2$. The pointwise magnitude of the surface tension force is proportional to σ/a and it is acting on the surface of the droplet giving a total force proportional to σa. The viscous force is proportional to $\mu_l \dot{x}/a^2$ and is integrated over the volume of the droplet adding an additional factor of a^3 resulting in an expression for the force proportional to $\mu_l \dot{x} a$. A constant is assigned to each term that accounts for the omitted constants in the above considerations and to allow for matching the model to measured data.

The oscillation amplitude, x, is made dimensionless by relating it to the droplet radius,

$$y = \frac{x}{C_b a}, \tag{3}$$

where C_b is chosen such that the droplet breaks when y exceeds unity.

By inserting Eqs. (2) and (3) into Eq. (1) a dimensionless equation for the oscillation is obtained,

$$\ddot{y} = \frac{C_F}{C_b}\frac{\rho_g}{\rho_l}\frac{u_r^2}{a^2} - \frac{C_k\sigma}{\rho_l a^3}y - \frac{C_d\mu_l}{\rho_l a^2}\dot{y}. \tag{4}$$

By assuming constant relative velocity u_r the equation can be solved, giving

$$y(t) = A + \exp\left(-\frac{t}{t_d}\right)\left|(y_0 - A)\cos(\omega t) + \frac{1}{\omega}\left(\dot{y}_0\frac{y_0 - A}{t_d}\right)\sin(\omega t)\right|, \tag{5}$$

where

$$A = \frac{C_F}{C_k C_b}\frac{We_g}{2}, \qquad We_g = 2\frac{\rho_g u_r^2 a}{\sigma}, \qquad t_d = \frac{2}{C_d}\frac{\rho_l a^2}{\mu_l}, \qquad \omega^2 = C_k\frac{\sigma}{\rho_l a^3} - \frac{1}{t_d^2}, \tag{6}$$

and y_0 and $\dot{y}_0$ are the initial conditions for the amplitude of the oscillation and its derivative, respectively.

In this work they are both assigned to the value 0. Note that the Weber number, We_g, is defined here with the droplet diameter rather than the radius as in the original paper [1].

Large viscosity modification

The stability limit of a low viscosity droplet has been determined experimentally to be $We_g = 12$. For viscous fluids it is larger and the effect of viscosity on the stability limit has been studied by Brodkey [7]. He came up with an empirical relation taking the viscosity into account by introducing the Ohnesorge number,

$$Oh = \frac{\mu}{\sqrt{2\rho_l \sigma a}}, \tag{7}$$

a dimensionless number relating the viscous force to the inertial and surface tension forces. Brodkey's empirical relation is expressed as

$$We_{g,crit} = 12\left(1 + 1.077Oh^{1.6}\right). \tag{8}$$

We see that in the limit of small Ohnesorge numbers, valid for $Oh \lesssim 0.1$, the above value of the critical Weber number is recovered. In viscous fluids, however, we see that the stability limit is increased and scales as $\mu^{1.6}$ in the asymptotic limit. What is more interesting, perhaps, is that the Ohnesorge number introduces the droplet diameter in the stability criterion. That is, smaller droplets appear more stable than larger ones when exposed to the same Weber number. The scaling of the stability limit with the size of the droplet is $1/a^{0.8}$ in the asymptotic limit.

Following Schmehl et al. [8] an effective Weber number is introduced, written as

$$We_g^{eff} = \frac{We_g}{1 + 1.077Oh^{1.6}}. \tag{9}$$

This effective Weber number is used in place of the regular one in Eq. 6 when simulations are performed with the modified TAB model.

Breakup event modeling

There are now three free parameters that need to determine: C_F/C_b, C_k, and C_d. In addition, the size of the resulting droplets of a breakup event needs to be modeled. To do this, a balancing of energy before and after the breakup event is performed. In the frame of reference of the droplet the available energy before the breakup is the sum of the contributions from the surface tension and from the oscillating motion. It is assumed that child droplets are not oscillating immediately after the breakup so that their energy is stored only in the surface tension. Together with the mass conservation constraint this gives an equation for the number of child droplets and their radius. A distribution of droplet radii seems more physically plausible, and therefore the child droplet radius is drawn from a Rosin-Rammler [9] distribution centered at the radius obtained as described above. This gives us two more parameters to be determined: the scale and shape parameters of the distribution, λ and k.

Flow solver

The flow solver IBOFlow [4] used to solve for the air flow is an incompressible, segregated Navier-Stokes solver. It is based on a collocated finite volume discretization on a Cartesian octree grid with cubic cells that is automatically generated and dynamically refined/coarsened based on static or adaptive rules. Internal boundaries that may be moving and interacting with the flow are efficiently handled through unique immersed boundary methods [4, 10].

Lagrangian particle tracking

Paint droplets are treated as Lagrangian particles that are traced in the fluid flow field. The equation of motion is written

$$m_p \ddot{\mathbf{r}} = \mathbf{F}_d\left(\mathbf{u}_r\right) \tag{10}$$

subject to the initial conditions $\mathbf{r}(0) = \mathbf{r}_0$ and $\dot{\mathbf{r}}(0) = \mathbf{v}_0$, where $\mathbf{r}$ is the particle position, $\mathbf{r}_0$ its initial position and $\mathbf{v}_0$ is the initial velocity. The force acting on the particle is the sum of the buoyancy and the drag forces,

$$\mathbf{F}_d = \mathbf{g}\left(\rho_p - \rho_g\right)V_p - \mathbf{u}_r|\mathbf{u}_r|C_d\frac{3}{4}\frac{\rho_g}{\rho_p}\frac{m_p}{2a}, \tag{11}$$

where $\mathbf{g}$ is the gravitational acceleration and V_p is the volume of the particle. The drag coefficient is evaluated according to the expression of Schiller and Neumann [11]

$$C_d = 24\frac{1 + 0.15Re_p^{0.687}}{Re_p}, \qquad Re_p = \frac{2a|\mathbf{u}_r|\rho_g}{\mu_g}, \tag{12}$$

where μ_g is the dynamic viscosity of the gaseous phase.

The equation of motion is efficiently solved for each droplet by the CVODE [12] solver from the Sundials [13] software package for numerical solution of differential and algebraic equations.

Numerical modeling

Paint

The paint is injected into the air by a rotating bell, see Fig. 2. The paint enters from the center of the bell and is then pushed outwards by the centrifugal force. At the edge there are serrations that act like tiny channels for the paint. The paint therefore enters the air as filaments extending a few millimeters in the radial direction away from the bell edge. A snapshot of the breakup region is displayed in Fig. 3. As the TAB model is not intended to

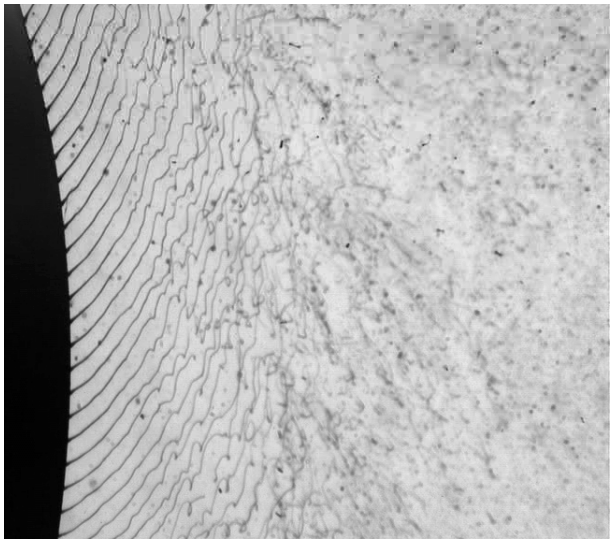

Figure 3. Filaments of paint at the bell edge seen to the left in the picture are rotating with a tangential velocity directed downwards. The filaments stay intact for a few millimeters and then break into non-spherical droplets. Courtesy of Swerea IVF.

model filament breakup we have to set up a model of the primary breakup that can be used as input to the TAB model. What can be modeled are the initial size and velocity distributions, and the position of the particles. The assumption is that the fingers break into fairly large fragments that subsequently break further. The filaments also slow down with respect to the air due to the drag force from the large relative velocity to the air. The diameter of the injected particles is modeled as log-normally distributed with mean and standard deviation equal to 100 and 50 μm, respectively. The initial velocity is uniformly distributed with a maximum equal to the velocity of the bell edge and a minimum half of it.

The viscosity of the paint has been measured to approximately 120 cP, or 0.12 Pa·s with a Ford viscosity cup #4 [14, Sec. 2.2.4]. The paint is a non-Newtonian liquid, but the viscosity is constant at shear rates $\gtrsim 500$ s^{-1}. The shear rate is expected to be at least this large during the breakup process, and the paint is therefore treated as a Newtonian liquid with the above given viscosity. The surface tension coefficient is measured to be 0.025 N/m, and the density is 995 kg/m^3. The paint flow rate is 330 cc/min.

Air

The shaping air is injected through two rings of circular nozzles of diameter approximately 1 mm, located above the bell and directed downwards towards the bell edge. These nozzles are too small to resolve as it would require huge amount of computational cells. Instead, an annulus is used as inlet condition for the air. The inlet condition is set such that the flow of momentum through the annulus is equal to that of the nozzles on the real

applicator. The mass flow is larger, however, as surrounding air is entrained as the jets from the air injection nozzles slow down. The annulus has an inner radius of 35 mm and outer radius 39 mm. The air velocity is 35 m/s directed downwards. These values correspond to a shape air of 260 slpm (standard liters per minute).

Simulation setup

The bell is modeled as a cut off cone with dimensions to match those of the bell seen in Fig. 1. The base diameter is 5.5 cm, top diameter 3.375 cm and height 2.5 cm. The shape air injection is placed just behind the bell as an annulus located 0.5 cm below the top of the bell with inner diameter 7.0 cm and outer diameter 7.8 cm. The robot head is modeled as a cut off cone placed right above the air injection plane. Its lower diameter is 10 cm and the cone angle is 106^o. Downdraft present in a paint booth is modeled as air injection on the upper boundary with a speed of 0.38 m/s directed downwards. The bottom boundary is an outlet and the four sides are modeled with symmetry boundary conditions allowing no flow in the normal direction. See Fig. 4 for a schematic description of the model. The bell boundary condition is set to zero rotation velocity as the boundary layer created by the bell

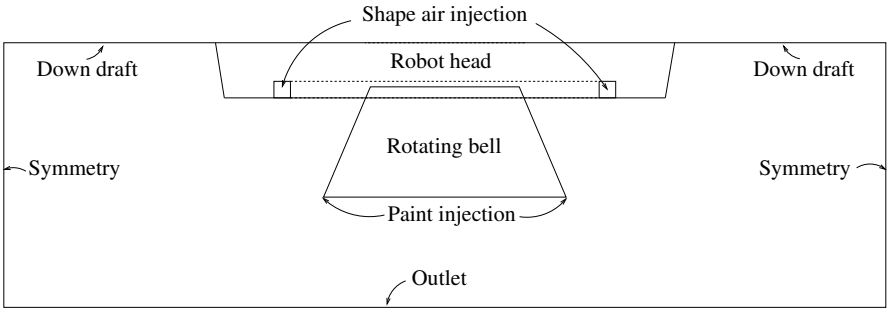

Figure 4. Schematic description of the setup of the simulation. The simulations are performed in three spatial dimensions and a cut through the center is shown. The simulation box is shown smaller than its actual size.

rotation is actually very thin, and does not extend past the primary breakup region. Instead, the swirling motion is created by the paint itself and the simulation is therefore performed with two-way coupled particles during the setup phase. During this phase correct size distributions are injected given the bell rotation speed, and a steady state solution is saved for each case considered. These solutions are later loaded in the optimization loop, where only one-way coupled simulations in a stationary air field are performed due to computational cost.

The mesh consists of Cartesian cubic cells in an octree structure. That means that cells can be refined by splitting them in eight new cells, doubling the resolution in each step. The base grid is built with 30x30x10 cells with side length 20 mm. It is refined five times at the surface of the bell, so that the resolution is $20/2^5 = 0.625$ mm. The thickness of this refinement region is 3.1 mm. The base mesh is connected by a series of refinements one, two, three and four times towards the inner finest region. The total thickness of the refined layer is approximately 10 cm. In addition, the shape air injection zone is refined three times and a hollow cylindric region below the bell edge is refined four times. In total $4.2 \cdot 10^5$ cells are created by this refinement.

The time step used in the flow solver is such that the CFL number equals 1. For 40 kRPM bell rotation speed this amounts to $7.2 \cdot 10^{-6}$ s. The particle time stepping uses an internal time step where the CFL is at most 0.5. In one time step between 50 and 150 primary droplets depending on their size are randomly distributed along the periphery of the bell's lower edge.

At injection each simulated droplet corresponds to exactly one physical droplet, but after breakup the simulated droplets correspond to many physical droplets each. This is done via a so-called cloud factor that determines the ratio of simulated droplets to physical ones. Its value is determined by matching the mass of the simulated droplet to the corresponding physical ones. A screen capture of the bell, air velocity and paint droplets is shown in Fig. 5

Measurement technique

The measurements were performed with a Spraytec RTS 5001 from Malvern Instruments [15] at the Fraunhofer-Institut für Produktionstechnik und Automatisierung (IPA) in Stuttgart, Germany. The measurement technique relies on Mie scattering where laser light is scattered by the droplets and the scattering angle differs depending on the droplet radius. An array of detectors detecting particles of different size are used to create a histogram of the sizes of droplets present in the spray. The spray is directed towards the measurement zone in such a way that all droplet sizes present in the spray pass by the detector and the obtained probability density functions are valid for the whole spray.

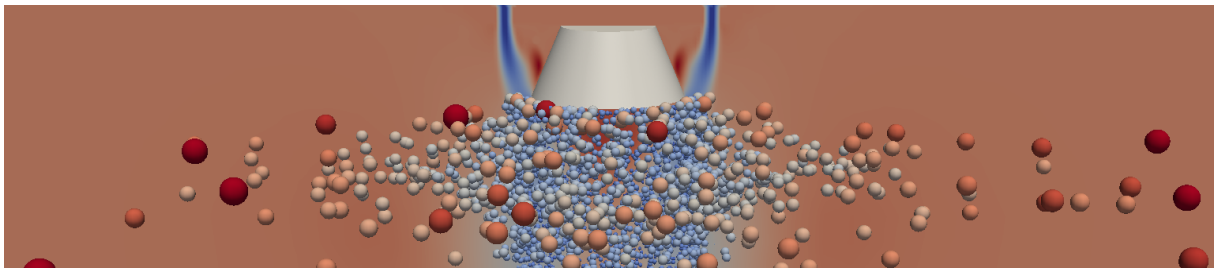

Figure 5. Screen capture of the simulation. The color scale of the droplets is according to their radii. The droplets are not shown in their real size but substantially larger as they would otherwise be too small to display. The cut plane through the 3D domain shows the downward air velocity.

Parameter estimation

The question of finding appropriate values for the coefficients of the models such that the simulated distributions match the measurements is treated as an optimization problem,

$$\min_{\mathbf{c}\in\mathbf{C}} F(\rho_s(\cdot;\mathbf{c}),\rho_m(\cdot)). \tag{13}$$

Here $\mathbf{c}$ is the vector of coefficients to the model, F is the objective function, $\rho_s(a;\mathbf{c})$ is the simulated size distribution, and $\rho_m(a)$ the measured one. The argument a to the distributions is droplet radius as before. As objective function the discrete normalized L^2 error is used,

$$F(\rho_s(\cdot;\mathbf{c}),\rho_m(\cdot)) = \left(\sum_{i=0}^{N}\left(\frac{\rho_s(a_i;\mathbf{c})}{\max_a \rho_s(a;\mathbf{c})} - \frac{\rho_m(a_i)}{\max_a \rho_m(a)}\right)^2\right)^{\frac{1}{2}}, \tag{14}$$

where the sample points a_i range over the support of the measured distribution and are logarithmically spaced to capture the appearance of the distributions. $N = 8192$ was used in this work.

The simulated droplet size distribution, ρ_s, is evaluated by running a simulation and extracted by so-called Kernel Density Estimate (KDE) as described by Botev et al. [16]. Their implementation [17] of the algorithm was slightly modified to work with logarithmically spaced data and to use a specified bandwidth. The confidence interval for the distribution decreases as $1/\sqrt{M}$ where M is the number of broken droplets in the simulation. This allows a trade off between accuracy and speed, where the simulation time in the optimization was chosen such that the difference between each set of parameters evaluated was statistically significant.

When the optimization of the parameters was initiated all five parameters, C_F/C_b, C_k, C_d, λ, and k were included as free variables. It became evident by studying response surfaces obtained by Radial Basis Functions (RBF) interpolation [18, 19], however, that the value of the damping coefficient C_d had negligible impact on the obtained size distributions by the model. As described in connection to Eq. 2 the C_d parameter determines how strongly the modeled harmonic oscillator is damped. It therefore enters the solution of the differential equation as the time constant for the oscillations, but does not otherwise affect the breakup. It does have a second order effect as larger values mean slower breakup that allows a longer time for the droplet to be slowed down relative to the air. The relative speed to the air at the moment of breakup affects the distribution of child droplets through the Weber number, but as mentioned earlier, this is a small effect for reasonable values of C_d. For this reason the standard value $C_d = 10$ was used and the number of variables in the optimization was reduced to four:

$$\mathbf{c} = [C_F/C_b, C_k, \lambda, k]^T. \tag{15}$$

As a starting point for the optimization, $\mathbf{c}_0$, the default values in KIVA 3 [2] were used. The four parameters are then allowed to vary in a four dimensional hypercube $\mathbf{c} \in \mathbf{C} = [\mathbf{c}_0/4, 4\mathbf{c}_0]$. The global optimization algorithm DIRECT [20] was used to solve the optimization problem in Eq. 13. To reach convergence a few hundred simulations were typically needed. Using an Intel Core i7-2600 processor running at 3.4 GHz with four parallel threads for the particle tracking required about one day to find a parameter set close to the global optimum.

Results

Parameters of the original TAB model in Eqs. 5-6 were tuned to match the measured size distributions at bell rotations speed of 30, 40 and 50 thousand revolutions per minute (RPM) simultaneously. Figure 6(a) shows the

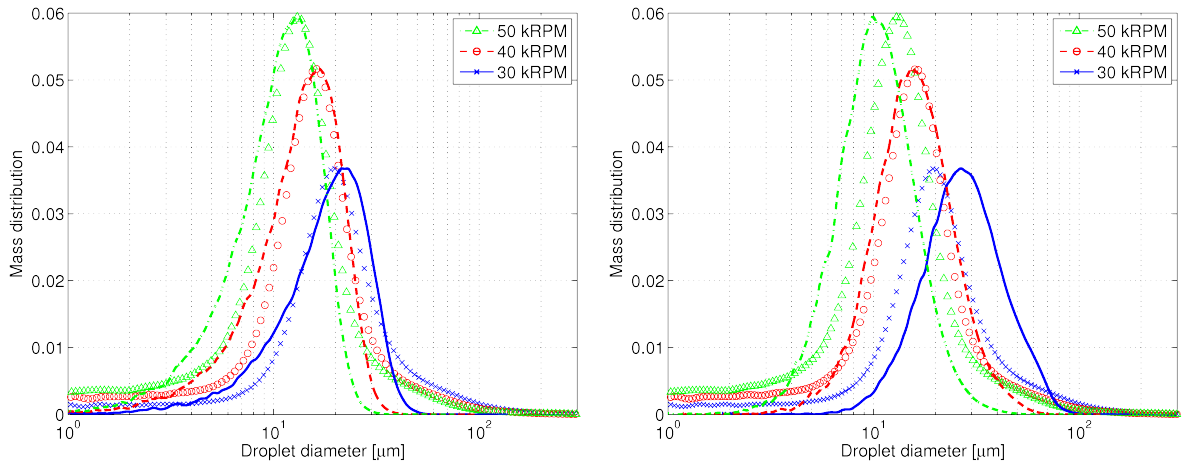

(a) Original TAB model (b) Large viscosity TAB model

Figure 6. Measured (markers) and simulated (lines) mass distribution as a function of droplet diameter. Simulated distributions are normalized to the maximum of the measured ones. Results for 30, 40 and 50 thousand RPM.

resulting measured and simulated distributions of mass as a function of droplet size. The broken droplets were sampled when their Weber number fell below 1, at which point it was determined that further breakup would not take place. Compare with the stability criterion in Eq. 8 which states $We = 12$ as the limit below which no breakup occurs. Using this criteria the breakup region extends only a few centimeters from the bell as the small droplets obtained after breakup are effectively decelerated, lowering the Weber number. The total simulation time was 0.2 s and around 10^6 primary droplets were injected during that time period. After breakup in the order of 10^9 droplets were recorded. As for the original TAB model, parameters of the model modified for large viscosity by using the definition of the effective Weber number in Eq. 9 were also optimized. The result is shown in Fig. 6(b).

We see that the simulations agree well with the measurements. The modes of the distributions are almost perfectly captured and the widths also fits well, except in the tails. A little bit too few large particles are retained in the simulation, and the small dust particles with diameters $\lesssim 5\mu$m are not entirely captured. The density of particles is very low in the tails in the measurements, however, which means that the mass present there is small. The main difference between the results of the original and modified TAB models is the slant of the distributions. The original model gives a steeper cut off at larger particles whereas the modified model gives a steeper distribution for smaller particles, and we see that the shape from the modified model fits better to the measurements. This difference can be explained by the introduction of the droplet diameter in the stability criterion by the Ohnesorge number. The optimal values of the parameters found are listed in Table 1.

Parameter	Original model	Modified model	KIVA 3 default
C_F/C_b	7.7829	23.1396	1.2051
C_k	5.7214	39.5628	4.66671
λ	13.0581	7.1598	0.95701
k	3.0745	5.4342	2.62501

Table 1. Optimal values obtained for the two TAB models by the optimization. The default value of the damping coefficient was used, $C_d = 10$.

Discussion and Conclusions

We have shown that the TAB model is able to capture the overall shape of the particle size distributions obtained by the rotary bell spraying technique. As the primary breakup is not included in the TAB model it has

to be accounted for separately. It does not, however, appear to be particularly sensitive to the initial distribution as it seems sufficient to use a crude model for the primary breakup. This is under the assumption that the primary breakup creates droplets of which a large fraction break during the secondary breakup, which is believed to be the case.

The tails of the distributions are less well captured, in both the upper and lower end. The distributions are slightly too narrow and as a consequence slightly over-estimate the density of particles in the middle of the distribution. In the upper end this could be due to collisions that are not included in the current study. This effect is believed to be small as the spray becomes progressively more dilute as droplets spread outwards.

The dependency on the rotational speed of the bell is somewhat over-estimated, especially by the modified model. The difference between the modes of the distributions in the measurements is slightly less than linear in rotation speed, which may be surprising. The simulations on the other hand scales slightly super-linearly.

Two-way coupled simulations were run during the initialization of the optimization problem, but one-way coupled simulations were performed in the actual optimization loop. This is primarily due to the computational cost of having to update the air solution each time step due to the back coupling from the droplets to the air. The error introduced by this simplification is believed to be small. A small widening of the simulated size distributions could be expected by running two-way coupled simulations due to fluctuations in the relative velocities.

By being able to simulate the droplet breakup the need for costly and cumbersome measurements is reduced. A limited set of measured droplet size distributions is needed for tuning the model, and it can then be used to predict changes in the size distributions without the need for new measurements. The obtained results are then used as input to full spray painting simulations that can be used by the automotive industry to reduce the time required for introduction of new car models, reduce the environmental impact and increase the quality.

Acknowledgements

This work has been conducted within the Virtual Paint Shop project. It was supported in part by the Swedish Governmental Agency for Innovation Systems, VINNOVA, through the FFI Sustainable Production Technology program, and in part by the Sustainable Production Initiative and the Production Area of Advance at Chalmers. The support is gratefully acknowledged. Henrik Karlsson at Swerea IVF is acknowledged for managing the measurement campaign giving the experimental results.

References

[1] O'Rourke P. J., Amsden A. A. *SAE paper 872089* (1987).
[2] Kiva 3, `http://www.lanl.gov/orgs/t/t3/codes/kiva.shtml`.
[3] Openfoam, `http://www.openfoam.com/`.
[4] Mark, A., Rundqvist, R., and Edelvik, F., *Fluid Dynamics & Materials Processing*, 7-3:241–258 (2011).
[5] Rundqvist, R., Mark, A., Andersson, B., Ålund, A., Edelvik, F., Tafuri, S., Carlson J. S., *Numerical Mathematics and Advanced Applications 2009*, Springer Berlin Heidelberg, 2010.
[6] Mark, A., Andersson, B., Tafuri, S., Engström, K., Söröd, H., Edelvik, F., Carlson, J. S., *12th International Conference on Liquid Atomization and Spray Systems*, Heidelberg, Germany, September 2012.
[7] Brodkey R. S., Addison-Wesley Series in Chemical Engineering, New York, NY, USA, 1967.
[8] Schmehl, R., Maier, G., Wittig, S., *8th International Conference on Liquid Atomization and Spray Systems*, Pasadena, CA, USA, July 2000.
[9] Rosin, P., Rammler, E., *Journal of the Institute of Fuel*, 7:29 – 36 (1933).
[10] Mark, A., van Wachem, B. G. M., *Journal of Computational Physics*, 227-13:6660 – 6680 (2008).
[11] Schiller, L. Neumann, A., *Ver. Deutsch. Ing.*, 77:318–320 (1933).
[12] Cohen, S. D., Hindmarsh, A. C., *Computers in Physics*, 10-2:138–143 (1996).
[13] Hindmarsh, A. C., Brown, P. N., Grant, K. E., Lee, S. L., Serban, R., Shumaker, D. E., Woodward, C. S., *ACM Trans. Math. Softw.*, 31-3:363–396 (2005).
[14] Viswanath, D.S., Springer (2007).
[15] Malvern Instruments, `http://www.malvern.com`.
[16] Botev, Z. I., Grotowski, J. F., Kroese, D. P., *Annals of Statistics*, 38(5):2916–2957 (2010).
[17] Botev, Z. I., `http://www.mathworks.com/matlabcentral/fileexchange/14034-kernel-density-estimator`.
[18] Wendland, H., Cambridge University Press, Cambridge (2005).
[19] Jakobsson, S., Patriksson, M., Rudholm, J., Wojciechowski, A., *Optimization and Engineering*, 11-4:501–532 (2010).
[20] Jones, D. R., Perttunen, C. D., Stuckman, B. E., *J. Optim. Theory Appl.*, 79:157–181 (1993).